# Slip Effects on Electrical Unsteady MHD Natural Convection Flow of Nanofluid over a Permeable Shrinking Sheet with Thermal Radiation

Yahaya Shagaiya Daniel, Zainal Abdul Aziz, Zuhaila Ismail, and Faisal Salah

*Abstract*—**The unsteady magnetohydrodynamic (MHD) natural convection flow and heat transfer of an electrical conducting incompressible viscous nanofluid over a linear permeable shrinking sheet in the presence of electric field, thermal radiation, viscous dissipation, chemical reaction, slip and passively controlled conditions at the wall is studied. The boundary layer governing equations which are partial differential equations are converted into a system of nonlinear ordinary differential equations by applying a suitable similarity transformation. Implicit finite difference scheme is applied to investigate the numerical results how the various physical embedded parameters affect the nanofluid flow and heat transfer with the aid of different graphical presentations and tabular forms. The nanofluid flow is due to a decelerating shrinking sheet as the electric field reduced the nanofluid velocity, and the first solution is stable compared to the second solution. Thermal radiation and viscous dissipation boost the nanofluid temperature whereas thermal slip reduces. Thermal convective parameter and mass convective parameter demonstrated opposite behavior. The magnetic field, unsteadiness parameter, and the suction parameter widen the range for the solution existence. Comparisons with previously published works seen in literature were performed and found to be in excellent agreement.**

*Index Terms*—**Magnetic nanofluid, unsteady flow, shrinking sheet, suction, dual solutions, thermal radiation**

## I. Introduction

THE conventional heat transfer fluids due to poor nature of thermal conductivity cannot meet up with the expectations and requirement for cooling rate. As such leads to a new class of fluid known as nanofluid. It is colloidal suspensions of ultrafine nanoparticles into a base fluid. The application of additives enhance the convective heat transfer performance of the conventional fluids and also increase the thermal conductivity.

Magnetic nanofluid contains the fluid and magnetic nanoparticle, features as result of its uniqueness. It plays a vital role as results of broad applications such as the processing of fusing metals due to the electric furnace through a magnetic field, and cooling of the initial plate enclosed nuclear reactor involving vessel where the hot plasma is separated from the plate by means of the magnetic field [1-11]. The nanofluids can be enriched through engineering system by different techniques involving plasma, synthesis and sheet processing. Some of these applications via aerodynamic extrusion of plastic sheets, the boundary layer against fluid film enclosed condensation mechanism and heat treated material that flows between wind-up rolls and feed, cooling of metallic wall seen in cooling bath, the boundary layer against material handling conveyors. The innovative work of Choi and Eastman [12], the enhancement of convective heat transfer according to Buongiorno [13] assumed that the volume fraction of nanoparticles in the nanofluid may not be uniform. Buongiorno [13] developed a two-phase model for convective transport in nanofluids incorporated the effects of Brownian motion and thermophoresis. Tiwari and Das [14] considered that thermophysical properties were viewed as functions of nanoparticle volume. After these mentioned works, different researchers have explored on nanofluid [15-25] due to its substantially significant and applications.

Boundary layer flow due to shrinking sheet in connection with nanofluid is an important type of flows as results of its crucial role. Conversely to stretching sheet, the shrinking case, the flow on the boundary is towards a fixed point, for instance, transforms the loose sleeves are wrapping of plastic that firmly fit into the shape of the sealed off contains in shrinking sheet, and rising and shrinking balloon. It is designed for various kinds of materials involving shrinking transparency, different strength, and luster. There are two conditions that the flow due to shrinking sheet can be noticed such as adequate suction [26] on the boundary or stagnation flow [27] so that the flow of the shrinking sheet is confined in the boundary layer. There is an extensive

Manuscript received Feb 02, 2017; revised Aug 09, 2017. (Submitted Oct. 09, 2017.) This work was supported by Ministry of Higher Education and Research Management Centre.

Y.S. Daniel is a Postgraduate student with the Department of Mathematical Sciences, Faculty of Science, Universiti Teknologi Malaysia, 81310 UTM Johor Bahru, Johor, Malaysia (e-mail: shagaiya12@gmail.com).

Z. A. Aziz is a Professor of Applied Mathematics and Director of the UTM Centre for Industrial and Applied Mathematics, Institute Ibnu Sina for Scientific and Industrial Research, 81310 UTM Johor Bahru, Johor, Malaysia (e-mail: zainalaz@utm.my).

Z. Ismail is a Senior Lecturer and staff member in the UTM Centre for Industrial and Applied Mathematics, Institute Ibnu Sina for Scientific and Industrial Research, 81310 UTM Johor Bahru, Johor, Malaysia (corresponding author phone number: +60 19-473 4003; e-mail: zuhaila@utm.my).

F. Salah is Assoc. Professor at the Department of Mathematics, Faculty of Science, University of Kordofan Elobied, 51111, Sudan (e-mail: faisal19999@yahoo.com).

literature material on the boundary layer flow against shrinking sheet as result of its modern industrial applications [28-34]. It has been extensively used in different engineering fields and industries for expanding and contracting of surfaces via shrinking wrapping, hot rolling, bundle wrapping, wire rolling, extrusion of sheet material and glass fiber.

The aim of the present investigation is to study the flow and heat transfer problem of unsteady MHD natural convection flow and heat transfer, a two-dimensional laminar flow of a viscous nanofluid due to a linear permeable shrinking sheet, with slip effects in the presence of electric field, thermal radiation, viscous dissipation, and chemical reaction. The momentum and energy fields at the wall are the slip conditions. The no-slip assumption is inconsistent with physical behavior that is more practically flow situations. It is of paramount importance to replace the no-slip boundary condition with partial slip conditions. The nanoparticle volume fraction on the boundary is passively controlled rather than actively [35]. The combination of nanoparticles and conventional fluids depends on the intention and purpose, our base fluid is water [17]. In the analysis, the constitute boundary layer governing equations have been converted to a two-point boundary layer value problem with the aids of defined similarity variables. The resultant nonlinear ordinary differential equations are solved using implicit finite difference scheme known as Keller box method [36]. The impacts of the entrenched physical parameters on the nanofluid velocity, temperature and concentration have been discussed and displayed in graphs and tables. Unlike stretching sheet, the solutions for shrinking sheet are not unique. Furthermore, the combined effects of the embedded parameters on the boundary layer flow and heat transfer due to nanofluid have been examined. Based on the author's knowledge, the present investigation is of essential values in the modern industries and not earlier reported in the literature.

## II. MATHEMATICAL FORMULATION

Consider the unsteady electrical magnetohydrodynamic (MHD) natural convective, two-dimensional incompressible electrically conducting viscous and laminar flow of a water-based nanofluid over a permeable shrinking sheet in the presence of thermal radiation, viscous dissipation, and chemical reaction. The flow is subjected to applied electric and magnetic fields $E$ and $B$ which are assumed to be applied in the direction $y>0$, normal to the surface see Fig. 1. The electric and magnetic fields confirm the Ohm's law $J=\sigma\left(E+V\times B\right)$, where $J$ stand for the Joule current, $V$ is the fluid velocity and $\sigma$ denote the electrical conductivity. The induced magnetic field and Hall current impacts are overlooked due to small magnetic Reynolds number. The velocity of the linearly shrinking sheet is assumed in the form $\varepsilon u_w\left(x,t\right)$, where $\varepsilon<0$ for a shrinking sheet and the velocity of the mass transfer denoted $v_w\left(t\right)$, here $x-$ and $y-$ axes are measured along the shrinking sheet and $t$ are the time. It is also assumed that the temperature at the surface of the sheet denoted by $T_w$ and the ambient temperature and concentration denoted by $T_\infty$ and $\varphi_w$ respectively. Using the Buongiorno model with aforementioned assumptions, the boundary layer governing equations are expressed as follows:

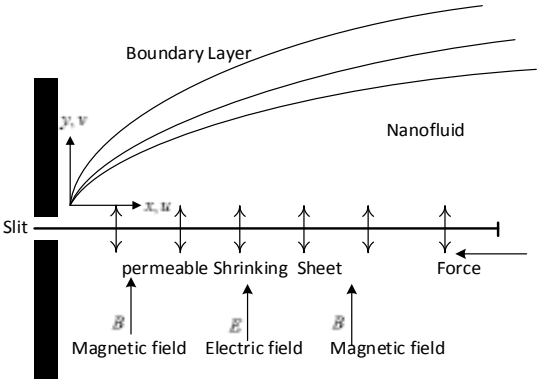


**Fig. 1** Physical configuration of the geometry

Continuity equation

$$\frac{\partial v}{\partial x}+\frac{\partial u}{\partial y}=0 \tag{1}$$

$x-$ Momentum equation

$$\frac{\partial u}{\partial t}+u\frac{\partial u}{\partial x}+v\frac{\partial u}{\partial y}=-\frac{1}{\rho_f}\frac{\partial p}{\partial x}+\nu\left(\frac{\partial^2 u}{\partial x^2}+\frac{\partial^2 u}{\partial y^2}\right)+\frac{\sigma}{\rho_f}\left(EB-B^2u\right)+\left[\left(1-\varphi_\infty\right)\beta_T\left(T-T_\infty\right)+\frac{\left(\rho_p-\rho_f\right)}{\rho_f}\beta_\varphi\left(\varphi-\varphi_\infty\right)\right]g \tag{2}$$

$y-$ Momentum equation

$$\frac{\partial v}{\partial t}+u\frac{\partial v}{\partial x}+v\frac{\partial v}{\partial y}=-\frac{1}{\rho_f}\frac{\partial p}{\partial y}+\nu\left(\frac{\partial^2 v}{\partial x^2}+\frac{\partial^2 v}{\partial y^2}\right)+\frac{\sigma}{\rho_f}\left(EB-B^2v\right)+\left[\left(1-\varphi_\infty\right)\beta_T\left(T-T_\infty\right)+\frac{\left(\rho_p-\rho_f\right)}{\rho_f}\beta_\varphi\left(\varphi-\varphi_\infty\right)\right]g \tag{3}$$

Energy equation

$$\frac{\partial T}{\partial t}+u\frac{\partial T}{\partial x}+v\frac{\partial T}{\partial y}=\frac{k}{\left(\rho c\right)_f}\left(\frac{\partial^2 T}{\partial x^2}+\frac{\partial^2 T}{\partial y^2}\right)+\frac{\mu}{\left(\rho c\right)_f}\left(\frac{\partial u}{\partial y}\right)^2-\frac{1}{\left(\rho c\right)_f}\frac{\partial q_r}{\partial y}+\tau\left\{D_B\left(\frac{\partial\varphi}{\partial x}\frac{\partial T}{\partial x}+\frac{\partial\varphi}{\partial y}\frac{\partial T}{\partial y}\right)+\frac{D_T}{T_\infty}\left[\left(\frac{\partial T}{\partial x}\right)^2+\left(\frac{\partial T}{\partial y}\right)^2\right]\right\} \tag{4}$$

Concentration equation

$$\frac{\partial\varphi}{\partial t}+u\frac{\partial\varphi}{\partial x}+v\frac{\partial\varphi}{\partial y}=D_B\left(\frac{\partial^2\varphi}{\partial x^2}+\frac{\partial^2\varphi}{\partial y^2}\right)+\frac{D_T}{T_\infty}\left(\frac{\partial^2 T}{\partial x^2}+\frac{\partial^2 T}{\partial y^2}\right)-k_1\left(\varphi-\varphi_\infty\right) \tag{5}$$

The boundary conditions at the sheet for the physical model are presented by

$$y=0: u=\varepsilon u_w\left(x,t\right)+l_1\frac{\partial u}{\partial y}, v=v_w\left(t\right), T=T_w\left(x,t\right)+l_2\frac{\partial T}{\partial y},$$

$$D_B\frac{\partial\varphi}{\partial y}+\frac{D_T}{T_\infty}\frac{\partial T}{\partial y}=0$$

$$y\to\infty: u=0, T\to T_\infty, \varphi\to\varphi_\infty \tag{6}$$

Here $u_w\left(x,t\right)=bx/\left(1-at\right)$ denotes the velocity of the shrinking sheet, $v_w\left(t\right)=v_0/\left(1-at\right)$ is the wall mass transfer, when $v_w<0$ represent the injection $v_w>0$ indicates the suction. Where $u$ and $v$ stands for the velocity components along the $x-$ and $y-$ axes respectively. For $g$, $p$, $\alpha=k/\left(\rho c\right)_f$, $\mu$, $\rho$, $\rho_f$, and $\rho_p$ is the gravitational acceleration, the pressure, the thermal diffusivity, the

kinematic viscosity, the density, the fluid density and particles density respectively. We also have $l_1 = l_1^{'}\sqrt{1-at}$, $l_2 = l_2^{'}\sqrt{1-at}, D_B, D_T, \tau = (\rho c)_p/(\rho c)_f$ which represents the velocity slip factor, temperature slips factor, Brownian diffusion coefficient, the thermophoresis diffusion coefficient, the ratio between the effective heat transfer capacity of the ultrafine nanoparticle material and the heat capacity of the fluid and $k_1 = k_0/(1-at)$ is the rate of chemical reaction respectively.

The radiative heat flux $q_r$ via Rosseland approximation [7] is applied to equation (4), such that,

$$q_r = -\frac{4\sigma^*}{3k^*}\frac{\partial T^4}{\partial y} \tag{7}$$

Where $\sigma^*$ represent the Stefan-Boltzmann constant and $k^*$ denote the mean absorption coefficient. Expanding $T^4$ by using Taylor's series about $T_\infty$ and neglecting higher order terms, we have,

$$T^4 \cong 4T_\infty^2 T - 3T_\infty^4 \tag{8}$$

Using equation (8) into (7), we get,

$$\frac{\partial q_r}{\partial y} = -\frac{16T_\infty^2}{3k^*}\frac{\partial^2 T}{\partial y^2} \tag{9}$$

Use equation (9) in equation (4), we have,

$$\frac{\partial T}{\partial t}+u\frac{\partial T}{\partial x}+v\frac{\partial T}{\partial y} = \frac{k}{(\rho c)_f}\left(\frac{\partial^2 T}{\partial x^2}+\frac{\partial^2 T}{\partial y^2}\right)+\frac{\mu}{(\rho c)_f}\left(\frac{\partial u}{\partial y}\right)^2+\frac{1}{(\rho c)_f}\left(\frac{16T_\infty^2\sigma^*}{3k^*}\frac{\partial^2 T}{\partial y^2}\right)+$$
$$\tau\left\{D_B\left(\frac{\partial \varphi}{\partial x}\frac{\partial T}{\partial x}+\frac{\partial \varphi}{\partial y}\frac{\partial T}{\partial y}\right)+\frac{D_T}{T_\infty}\left[\left(\frac{\partial T}{\partial x}\right)^2+\left(\frac{\partial T}{\partial y}\right)^2\right]\right\} \tag{10}$$

Using the order of magnitude analysis for the $y-$ direction momentum equation which is normal to the shrinking sheet and boundary layer approximation [37], such as

$$u \gg v$$
$$\frac{\partial u}{\partial y} \gg \frac{\partial u}{\partial x}, \frac{\partial v}{\partial t}, \frac{\partial v}{\partial x}, \frac{\partial v}{\partial y} \tag{11}$$
$$\frac{\partial p}{\partial y} = 0$$

After the analysis, the boundary layer equations (1)-(5) are reduced to the following as:

$$\frac{\partial v}{\partial x}+\frac{\partial u}{\partial y} = 0 \tag{12}$$

$$\frac{\partial u}{\partial t}+u\frac{\partial u}{\partial x}+v\frac{\partial u}{\partial y} = -\frac{1}{\rho_f}\frac{\partial p}{\partial x}+\nu\left(\frac{\partial^2 u}{\partial y^2}\right)+\frac{\sigma}{\rho_f}\left(EB-B^2u\right)+$$
$$\left[(1-\varphi_\infty)\beta_T(T-T_\infty)+\frac{(\rho_p-\rho_f)}{\rho_f}\beta_\varphi(\varphi-\varphi_\infty)\right]g \tag{13}$$

$$\frac{\partial T}{\partial t}+u\frac{\partial T}{\partial x}+v\frac{\partial T}{\partial y} = \frac{k}{(\rho c)_f}\left(\frac{\partial^2 T}{\partial y^2}\right)+\frac{\mu}{(\rho c)_f}\left(\frac{\partial u}{\partial y}\right)^2+\frac{1}{(\rho c)_f}\left(\frac{16T_\infty^2\sigma^*}{3k^*}\frac{\partial^2 T}{\partial y^2}\right)+$$
$$\tau\left\{D_B\left(\frac{\partial \varphi}{\partial y}\frac{\partial T}{\partial y}\right)+\frac{D_T}{T_\infty}\left(\frac{\partial T}{\partial y}\right)^2\right\} \tag{14}$$

$$\frac{\partial \varphi}{\partial t}+u\frac{\partial \varphi}{\partial x}+v\frac{\partial \varphi}{\partial y} = D_B\left(\frac{\partial^2 \varphi}{\partial y^2}\right)+\frac{D_T}{T_\infty}\left(\frac{\partial^2 T}{\partial y^2}\right)-k_1(\varphi-\varphi_\infty) \tag{15}$$

The resulted equations are reduced into the dimensionless form by introducing the following dimensionless quantities [38-41].

$$\psi = \sqrt{\frac{b\nu}{1-at}}xf(\eta),\ \eta = y\sqrt{\frac{b}{\nu(1-at)}},\ \theta = \frac{T-T_\infty}{T_W-T_\infty},$$
$$\phi = \frac{\varphi-\varphi_\infty}{\varphi_\infty},\ T_W(x,t) = T_\infty + T_0\frac{bx}{2\nu(1-at)^2}, \tag{16}$$

The stream function $\psi$ can be defined as:

$$u = \frac{\partial \psi}{\partial y},\ v = -\frac{\partial \psi}{\partial x} \tag{17}$$

The equations of momentum, energy and nanoparticle concentration in dimensionless form become:

$$f''' + ff'' - f'^2 - \delta\left(f' + \frac{\eta}{2}f''\right) + M\left(E_1 - f'\right) + \lambda_T\theta + \lambda_M\phi = 0 \tag{18}$$

$$\frac{1}{\Pr}\left(1+\frac{4}{3}Rd\right)\theta'' + f\theta' - 2f'\theta - \delta\left(\frac{\eta}{2}\theta' + 2\theta\right) + Nb\phi'\theta' + Nt\theta'^2 + Ec\left(f''\right)^2 = 0 \tag{19}$$

$$\phi'' + \frac{Nt}{Nb}\theta'' + Scf\phi' - Sc\delta\frac{\eta}{2}\phi' - Sc\gamma\phi = 0 \tag{20}$$

The boundary conditions are given by

$$f = s,\ f' = \varepsilon + L_1 f'',\ \theta = 1 + L_2\theta',\ Nb\phi' + Nt\theta' = 0, \text{ at } \eta = 0$$
$$f' = 0,\ \theta = 0,\ \phi = 0, \quad \text{as} \quad \eta \to \infty \tag{21}$$

Here $f', \theta,$ and $\phi$ is the dimensionless velocity, temperature, and concentration respectively. We have the following parameters:

$\delta = a/b$ denote the unsteadiness parameter,

$L_1 = l_1^{'}\sqrt{b/\nu}$ is the velocity slip parameter,

$L_2 = l_2^{'}\sqrt{b/\nu}$ depicts the thermal slip parameter,

$\lambda_T = Gr/Re^2$ thermal convective parameter

$Gr = g\beta_T(1-\varphi_\infty)(T_w - T_\infty)l^3/\nu^2$ is the Grashof number,

$X = x/l$ is the dimensionless constant,

$\lambda_M = Gm/Re^2$ mass convective parameter

$Gm = g\beta_\varphi(\rho_p - \rho_f)\varphi_\infty l^3/\nu^2\rho_f$ stand for the mass Grashof,

$\Pr = \nu/\alpha$ represent the Prandtl number,

$Nb = (\rho c)_p D_B\varphi_\infty/(\rho c)_f\nu$ is the Brownian motion,

$Sc = \nu/D_B$ denote the Schmidt number,

$Nt = (\rho c)_p D_T(T_W - T_\infty)/(\rho c)_f\nu T_\infty$ is the thermophoresis,

$M = \sigma B_0^2/b\rho_f$ represent the magnetic field,

$E_1 = E_0/u_w B_0$ denote the electric field,

$Ec = u_W^2/c_P(T_W - T_\infty)$ indicate the Eckert number,

$s = v_0/\sqrt{\nu b}$ is the suction $(s>0)$/injection $(s<0)$ parameter,

$Rd = 4\sigma * T_\infty^3/k * k$ denote the radiation parameter,

$\gamma = k_0/b$ is the chemical reaction, for $\gamma > 0$ associates to destructive chemical reaction while $\gamma < 0$ corresponds to generative chemical reaction respectively. Where prime represents differentiation with respect to $\eta$.

The skin friction coefficient and the local Nusselt number are

$$c_f = \frac{\tau_W}{\rho u_w^2(x,t)}, \qquad Nu = \frac{xq_W}{k(T_W - T_\infty)}, \tag{22}$$

Where

$$q_W = -\left(\left(k + \frac{16T_\infty^2\sigma^*}{3k*}\right)\frac{\partial T}{\partial y}\right)_{y=0}, \qquad \tau_W = \mu\left(\frac{\partial u}{\partial y}\right)_{y=0}, \tag{23}$$

Here $\tau_w$ is the shear stress for the shrinking surface, $q_w$ is the surface heat flux, while $\mathrm{Re} = u_w l/\nu$ is the Reynolds number and $k$ the thermal conductivity of the nanofluid. For the local skin-friction coefficient and local Nusselt are presented in non-dimensional form as

$$\mathrm{Re}^{1/2} c_f = f''(0), \qquad Nu/\mathrm{Re}^{1/2} = -\left(1+\frac{4}{3}Rd\right)\theta'(0), \tag{24}$$

## III. RESULTS AND DISCUSSION

Following Cebeci and Bradshaw [36] the system of ordinary differential equations (18)-(20) subject to the boundary conditions (21) are solved numerically using implicit finite difference scheme known as Keller box method for different values of the parameters. It is worth mentioning that the step size $\Delta\eta$ along with the boundary layer thickness is selected rendering to the values of parameters. These calculations are repeated until convergence criteria are satisfied at $10^{-5}$ is used. The numerical values of the skin friction with the available published data by Yasin et al. [32], Bhattacharyya [42] and Dhanai et al. [43] are displayed in Tables 1 and 2. In Table 1 is the comparison of the numerical values for the skin friction $f''(0)$, whereas Table 2 supporting the existence of multiple solutions of the present study. The present computation scheme in some limiting sense to that of the previous investigation noticed a perfect agreement.

The effects of the sundry parameters due to the decelerating sheet $(\delta \le 0)$ on the velocity, temperature, and nanoparticle concentration are given in Figs. 2-17. Fig. 2 reveal the variation of magnetic field $M$ on the velocity profile $f'(\eta)$. The water-based nanofluid velocity along the shrinking sheet increases with $M$ in the first solution, whereas in the second solution its decreases. The nanofluid due to the resistive force associated with Lorentz force has the tendency to retard the flow of the nanofluid. Intense magnetic field contributes resistance to flow. Physically, the effect of magnetic field is such that it gives rise to Lorentz force in a direction which opposes the flow in either direction as such leads to a reduction in the nanofluid velocity. In Figs. 3 and 4 demonstrate the effects of electric field $E_1$ and unsteadiness parameter $\delta$ on the velocity profiles $f'(\eta)$. In the first solution, the water-based nanofluid velocity shrinkages with an increase in electric field and unsteadiness parameters towards the sheet surface. The second solutions, close to the wall the nanofluid velocity intensified with the electric field and along the surface, after some distance, it's weakening. The Lorentz force acts as accelerating body force which accelerates the flow behavior due to interaction with electrically conducting nanofluid. The unsteadiness parameter $\delta$ designates a reduction in both solutions near the sheet due to decelerating flow. This depicts that first solution is stable as related to the second solution. The effect of a suction parameter $s$ on the nanofluid velocity profile $f'(\eta)$ is portrayed in Fig. 5. In the first solution, the velocity is a decreasing function whereas in the second solution illustrates an increasing function. It means that augmentation of suction leads to more separation due to the dual solution on the water base nanofluid velocity with decelerating shrinking. In Fig. 6, the impact of velocity slip parameter $L_1$ on the nanofluid velocity profile $f'(\eta)$ is publicized. The profile reveals that the velocity produces resistance to flow of nanofluid by virtue of higher values of $L_1$ for both solutions however after some distance along the shrinking sheet second solution supplements for smaller values of $L_1$. These thicknesses are higher for the second solution than the associated thicknesses of the first solutions.

The effects of thermal radiation $Rd$, Eckert number $Ec$, thermal convective parameter $\lambda_T$, unsteadiness parameter $\delta$ and thermal slip $L_2$ parameter on the temperature profiles are displayed in Figs. 7-11. Figs. 7 and 8 established how the thermal radiation $Rd$ and Eckert number $Ec$ affects the nanofluid temperature profile $\theta(\eta)$. It is observed that the effect of thermal radiation enhances the water base nanofluid temperature for an increase in the values of thermal radiation $Rd$ and Eckert number $Ec$. The reason is a result of emission due to heat transfer in the boundary layer region with a magnitude of decelerating shrinking. Consequently, the thermal boundary layer becomes thicker in the second solution compared to the first solution. The variation of thermal convective parameter $\lambda_T$ on the nanofluid temperature profile $\theta(\eta)$ is revealed in Fig. 9. Temperature is an increasing function with thermal convective parameter for the case of the second solution whereas for the first solution there is an insignificant behavior on the water-based nanofluid. It's represents the relative strength of thermal buoyancy force to viscous force. Increases when thermal buoyancy force upsurge. This implies that thermal buoyancy force tends to accelerate the nanofluid temperature in the thermal layer region as result of high density. The thermal boundary layer thickness becomes larger for greater values of thermal convective parameter due to a decelerating shrinking sheet. Fig. 10 represent the result of unsteadiness parameter $\delta$ on the temperature profile $\theta(\eta)$. It worth noticed that the unsteadiness parameter gain the water base nanofluid temperature. The second solution amplified and after some distance away from the wall shrinkage, that is crossing over. The first solution is more stable to the second solution. In Fig. 11 exhibit the outcome of thermal slip parameter $L_2$ on the nanofluid temperature profile $\theta(\eta)$. Both solutions diminish for higher values of thermal slip parameter. Higher values of thermal slip parameters resulted to thinner thermal boundary layer thickness due to water-based nanofluid temperature.

The effects on thermophoresis parameter $Nt$, Brownian motion $Nb$, Lewis number $Le$, chemical reaction $\gamma$, mass convective parameter $\lambda_M$, and unsteadiness parameter $\delta$ on the nanoparticles concentration profiles $\phi(\eta)$ are presented in Figs. 12-17. In Fig. 12 unveil the variation of thermophoresis parameter $Nt$ on the concentration profile $\phi(\eta)$. It is noticed that along the surface of the shrinking sheet, distance away from the wall both solutions increases for higher values. Due to a decelerating shrinking sheet of the water base nanofluid, for larger values of thermophoresis parameter creates a greater mass flux that enhances the nanoparticle volume fraction profile. Brownian motion

parameter $Nb$ on the concentration profile $\phi(\eta)$ has a decreasing upshot see Fig. 13. In both solutions, it reduced along the surface for higher values of Brownian motion. The increment in Brownian motion parameter enhances the temperature which leads to the decrement in nanoparticle concentration profile of the water-based nanofluid. Thus, it tends to reduce the separating, due to the nanoparticle concentration at the wall is passively controlled by mass transfer parameter and decelerating shrinking sheet. In Fig. 14 illustrates the influence of Lewis number $Le$ on the concentration profile $\phi(\eta)$. It worth noticed that thermal boundary layer thickness is thicker to the solutal boundary layer thickness, which resulted in a reduction in the nanoparticle concentration of the water-based nanofluid. Lewis number denotes the ratio of the viscous diffusion rate to the molecular diffusion rate. Physically, deals with the virtual thickness of the momentum and concentration boundary layers. So, intense Lewis number substantially decreases solutal boundary layer thickness. This implies that there is a much faster viscous diffusion rate compared with nanoparticle mass diffusion rate. In the decelerating shrinking sheet due to increase in Lewis number, the concentration distribution decreases in both solutions (that is the first and second solutions). Figs. 15 and 16 are the impacts of chemical reaction $\gamma$ and mass convective parameter $\lambda_M$ on the concentration profiles $\phi(\eta)$. The nanoparticle concentration condenses with chemical reaction and mass convective parameter for higher values. It's represent the virtue strength of solutal buoyancy force to viscous force. Thus, higher values decrease solutal buoyancy force. This implies that viscous force tends to shrink the water base nanofluid flow in the solutal layer region. This is more pronounced in the second solution with an insignificant effect in the first solution. In Fig. 17 demonstrated the power of unsteadiness parameter $\delta$ on the nanoparticle concentration $\phi(\eta)$. In the second solution near to the wall it growths and after some distance along the sheet, surface reduces substantially for higher values of unsteadiness parameter within the water-based nanofluid and the shrinking sheet. While in the case of the first solution insignificant drops consequence due to a decelerating shrinking sheet and passively controlled behavior.

**Table 1**: Numerical values of shear stress at the wall $f''(0)$ for different values of a suction parameter when $M = 2,\ \lambda_T = \lambda_M = \delta = E_1 = L_1 = 0$ and $\varepsilon = -1$.

| $s$ | Ref [42] | Ref [32] | Present results |
|---|---|---|---|
| 1 | - | 1.6180 | 1.618034 |
| 2 | 2.414300 | 2.4142 | 2.414214 |
| 3 | 3.302750 | 3.3028 | 3.302776 |
| 4 | 4.236099 | 4.2361 | 4.236068 |
| 5 | - | - | 5.192582 |
| 6 | - | - | 6.162278 |
| 7 | - | - | 7.140055 |
| 8 | - | - | 8.123106 |
| 9 | - | - | 9.109772 |
| 10 | - | - | 10.09902 |

**Table 2**: Numerical values of shear stress $f''(0)$ for different values of $S$ and $M$ when $\lambda_T = \lambda_M = \delta = E_1 = L_1 = 0$ and $\varepsilon = -1$.

| $S$ | $M$ | First solution Ref[43] | Second solution Ref[43] | Present first solution | Present second solution |
|---|---|---|---|---|---|
| 3.0 | 0.01 | 2.622498 | 0.377503 | 2.622497 | 0.377503 |
| | 0.09 | 2.657584 | 0.342416 | 2.657584 | 0.342416 |
| | 0.25 | 2.724745 | 0.275255 | 2.724745 | 0.275255 |
| 4.0 | 0.01 | 3.734935 | 0.265065 | 3.734935 | 0.265079 |
| | 0.09 | 3.757840 | 0.242160 | 3.757840 | 0.242161 |
| | 0.25 | 3.802776 | 0.197224 | 3.802776 | 0.197224 |
| 5.0 | 0.01 | - | - | 4.793469 | 0.206546 |
| | 0.09 | - | - | 4.810844 | 0.189168 |
| | 0.25 | - | - | 4.845208 | 0.154792 |

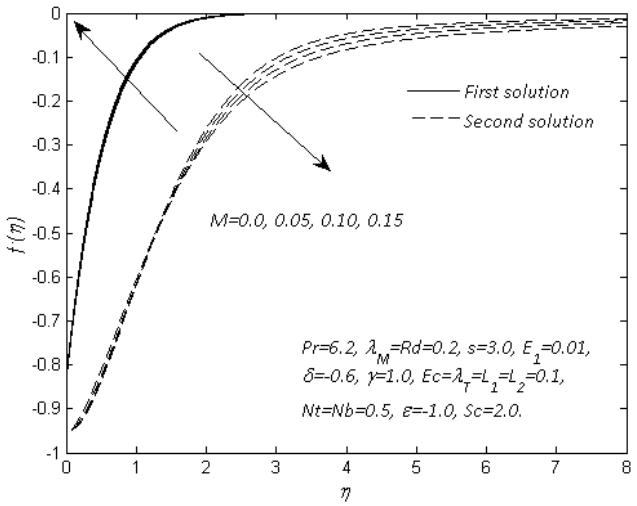


**Fig.2** Influence of $M$ on the velocity profile $f'(\eta)$

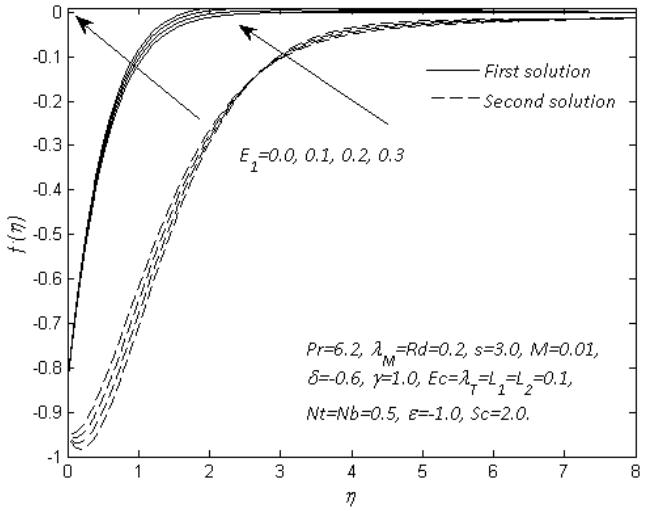


**Fig.3** Influence of $E_1$ on the velocity profile $f'(\eta)$

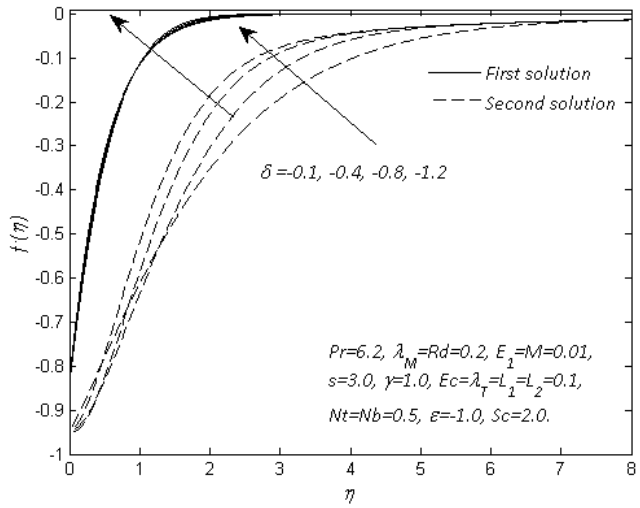


**Fig.4** Influence of $\delta$ on the velocity profile $f'(\eta)$

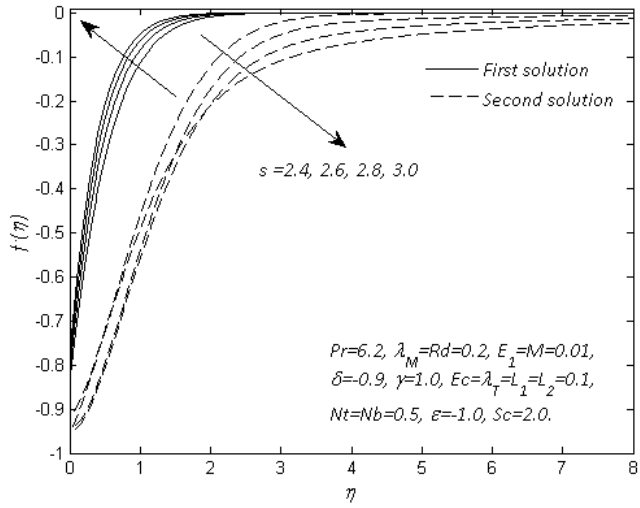


**Fig.5** Influence of $S$ on the velocity profile $f'(\eta)$

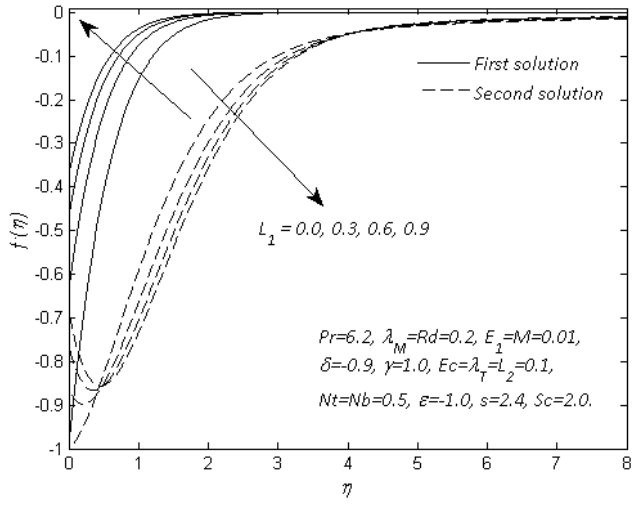


**Fig.6** Influence of $L_1$ on the velocity profile $f'(\eta)$

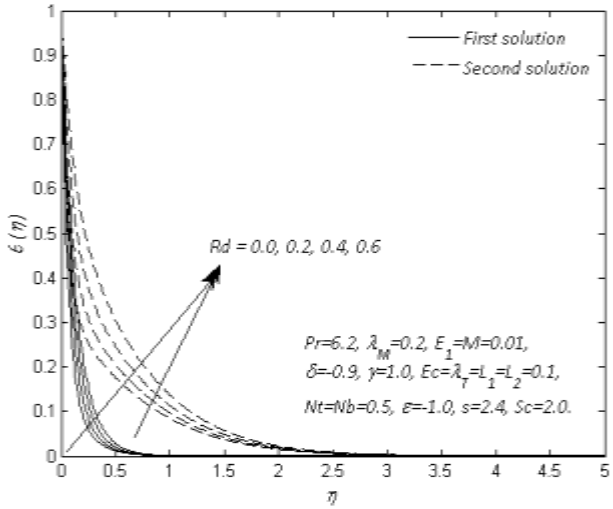


**Fig.7** Influence of $Rd$ on the temperature profile $\theta(\eta)$

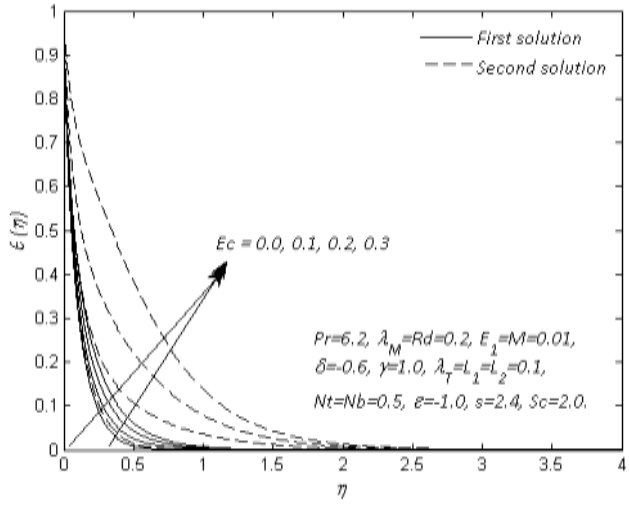


**Fig.8** Influence of $Ec$ on the temperature profile $\theta(\eta)$

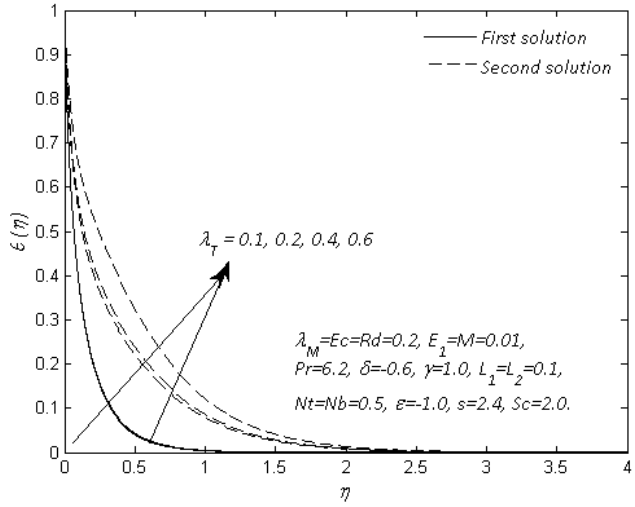


**Fig.9** Influence of $\lambda_T$ on the temperature profile $\theta(\eta)$

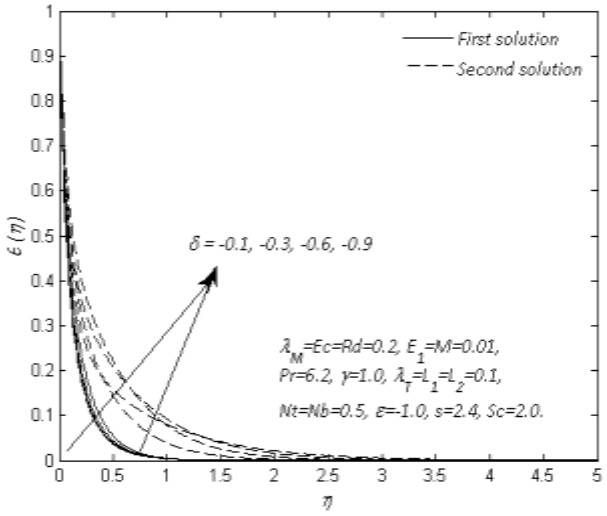


**Fig.10** Influence of $\delta$ on the temperature profile $\theta(\eta)$

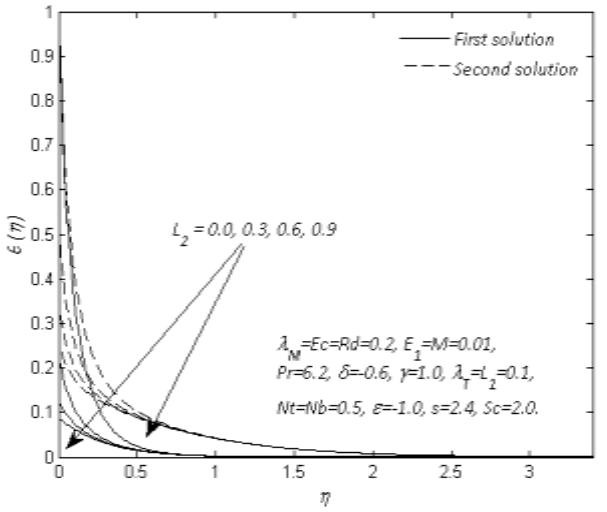


**Fig.11** Influence of $L_2$ on the temperature profile $\theta(\eta)$

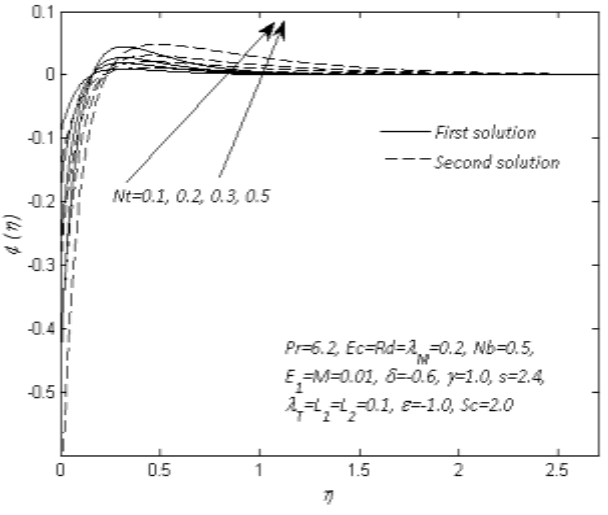


**Fig.12** Influence of $Nt$ on the concentration profile $\phi(\eta)$

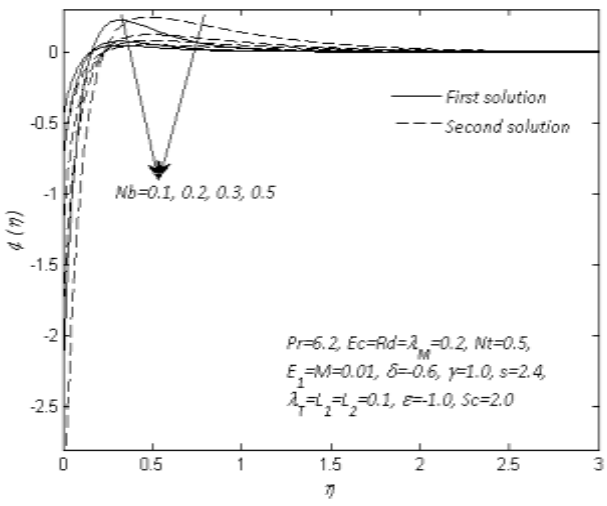


**Fig.13** Influence of $Nb$ on the concentration profile $\phi(\eta)$

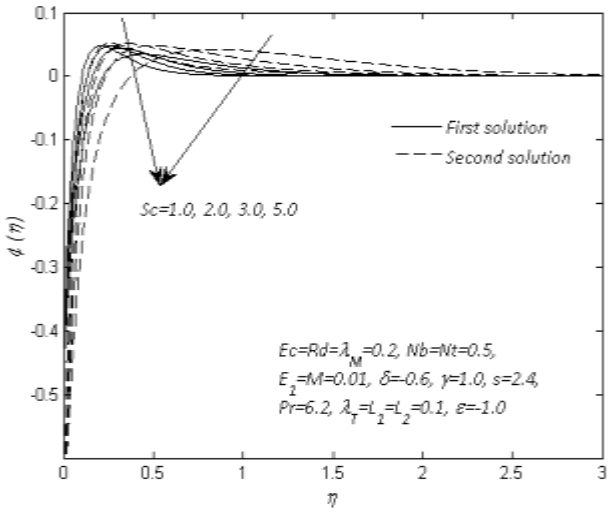


**Fig.14** Influence of $Sc$ on the concentration profile $\phi(\eta)$

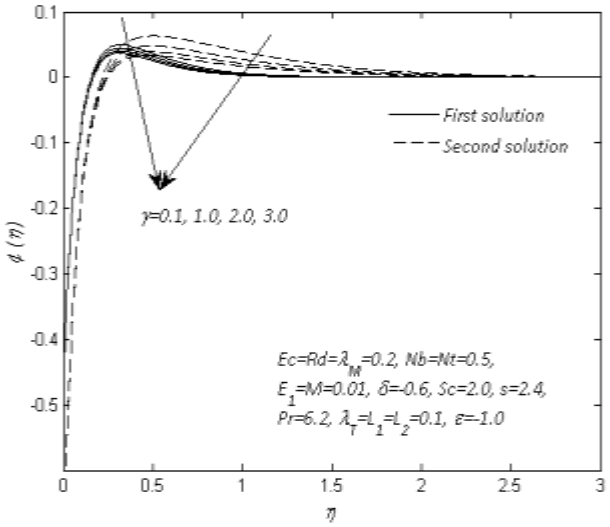


**Fig.15** Influence of $\gamma$ on the concentration profile $\phi(\eta)$

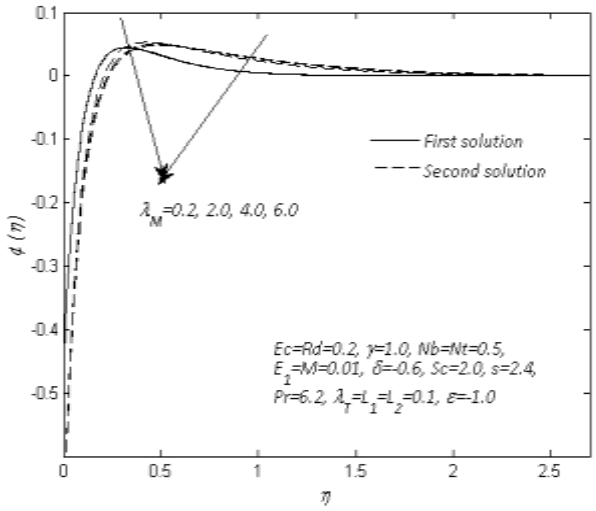


**Fig.16** Influence of $\lambda_M$ on the concentration profile $\phi(\eta)$

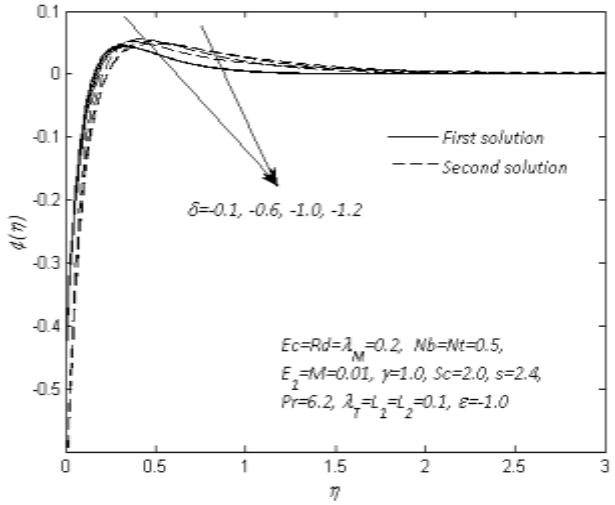


**Fig.17** Influence of $\delta$ on the concentration profile $\phi(\eta)$

## IV. CONCLUSION

The unsteady magnetohydrodynamic (MHD) natural convective flow of electrical conducting nanofluid over a permeable shrinking sheet in the presence of electric field, thermal radiation, viscous dissipation and chemical reaction with slips and passively controlled conditions at the wall are investigated. The decelerating shrinking sheet, slips and passively controlled conditions have been employed. The boundary layer governing the flow are partial differential equations are transformed into nonlinear ordinary differential equations and then solved numerically using implicit finite difference scheme. The effects of various physical parameters involved in the system of the equations namely: electric field, magnetic field, unsteadiness parameter, suction, velocity slip, thermal radiation, Eckert number, thermal convective parameter, thermal slip, thermophoresis, Brownian motion, Lewis number, mass convective parameter, and chemical reaction are obtained. The following conclusions are drawn in this investigation.

1. The effects of the wall suction and decelerating shrinking sheet revealed dual solutions.
2. The magnetic field, unsteadiness parameter, and the mass suction parameter widen the range of the solution existence.
3. Thermal radiation and Eckert number heighten the temperature and thermal boundary layer thickness.
4. The skin friction is sensitive to an increase in magnetic field and suction parameters.
5. Electric field and unsteadiness parameters decrease the velocity near the surface of the sheet, the first solution (upper solution branch) are stable to compare with the second solution (lower solution branch).
6. The thermal slip parameter reduces the nanofluid temperature and thermal boundary layer thickness in both solutions while opposite trend occurred with unsteadiness parameter.
7. Opposite behavior of the nanoparticle concentration is noticed with Brownian motion and thermophoresis parameters.
8. The thermal convective parameter and mass convective parameter exhibit opposite behavior whereas chemical reaction reduced the nanoparticle concentration with insignificant effect for the first solutions.

## ACKNOWLEDGMENT

The authors would like to express their sincere thanks to Ministry of Higher Education and Research Management Centre, UTM through GUP with vote number 11H90, Flagship vote number 03G50, 13H28 and 03G53 for this research.

## REFERENCES

[1] Z. Hedayatnasab, F. Abnisa, and W. M. A. W. Daud, "Review on magnetic nanoparticles for magnetic nanofluid hyperthermia application," *Materials & Design*, vol. 123, pp. 174-196, 2017.

[2] L. Mohammed, H. G. Gomaa, D. Ragab, and J. Zhu, "Magnetic nanoparticles for environmental and biomedical applications: A review," *Particuology*, vol. 30, pp. 1-14, 2017.

[3] Y. S. Daniel, Z. A. Aziz, Z. Ismail, and F. Salah, "Effects of slip and convective conditions on MHD flow of nanofluid over a porous nonlinear stretching/shrinking sheet," *Australian Journal of Mechanical Engineering*, pp. 1-17, 2017.

[4] S. Shabestari Khiabani, M. Farshbaf, A. Akbarzadeh, and S. Davaran, "Magnetic nanoparticles: preparation methods, applications in cancer diagnosis and cancer therapy," *Artificial cells, nanomedicine, and biotechnology*, vol. 45, no. 1, pp. 6-17, 2017.

[5] Y. S. Daniel, Z. A. Aziz, Z. Ismail, and F. Salah, "Entropy analysis in electrical magnetohydrodynamic (MHD) flow of nanofluid with effects of thermal radiation, viscous dissipation, and Chemical reaction," *Theoretical and Applied Mechanics Letters*, 2017. https://doi.org/10.1016/j.taml.2017.06.003

[6] Y. S. Daniel, Z. A. Aziz, Z. Ismail, and F. Salah, "Effects of thermal radiation, viscous and Joule heating on electrical MHD nanofluid with double stratification," *Chinese Journal of Physics*, vol. 55, no. 3, pp. 630-651, 2017.

[7] Y. S. Daniel and S. K. Daniel, "Effects of buoyancy and thermal radiation on MHD flow over a stretching porous sheet using homotopy analysis method," *Alexandria Engineering Journal*, vol. 54, no. 3, pp. 705-712, 2015.

[8] F. Ismagilov, I. Khayrullin, V. Vavilov, and A. Yakupov, "Generalized Mathematic Model of Electromechanical Energy Transducers with Non-contact Bearings," *Engineering Letters*, vol. 25, no. 1, pp. 30-38, 2017.

[9] Q. Duan, Y. L. Yang, and Y. Li, "Rough K-modes Clustering Algorithm Based on Entropy," *IAENG International Journal of Computer Science*, vol. 44, no. 1, pp. 13-18, 2017.

[10] Y. S. Daniel, "MHD Laminar Flows and Heat Transfer Adjacent to Permeable Stretching Sheets with Partial Slip Condition," *Journal of Advanced Mechanical Engineering*, vol. 4, no. 1, pp. 1-15, 2017.

[11] Y. S. Daniel, "Steady MHD Laminar Flows and Heat Transfer Adjacent to Porous Stretching Sheets using HAM," *American Journal of Heat and Mass Transfer*, vol. 2, no. 3, pp. 146-159, 2015.

[12] S. Choi and J. Eastman, "Enhancing thermal conductivity of fluids with nanoparticles. ASME International menchanical engineering congress and exposition," *American Society of Mechanical Engineers, San Francisco*, 1995.

[13] J. Buongiorno, "Convective transport in nanofluids," *Journal of Heat Transfer*, vol. 128, no. 3, pp. 240-250, 2006.

[14] R. K. Tiwari and M. K. Das, "Heat transfer augmentation in a two-sided lid-driven differentially heated square cavity utilizing nanofluids," *International Journal of Heat and Mass Transfer*, vol. 50, no. 9, pp. 2002-2018, 2007.

[15] Y. S. Daniel, "Presence of heat generation/absorption on boundary layer slip flow of nanofluid over a porous stretching sheet," *American J. of Heat and Mass Transfer*, vol. 2, no. 1, p. 15, 2015.

[16] C. Zhang, L. Zheng, X. Zhang, and G. Chen, "MHD flow and radiation heat transfer of nanofluids in porous media with variable surface heat flux and chemical reaction," *Applied Mathematical Modelling*, vol. 39, no. 1, pp. 165-181, 2015.

[17] F. Mabood, W. Khan, and A. M. Ismail, "MHD boundary layer flow and heat transfer of nanofluids over a nonlinear stretching sheet: a numerical study," *Journal of Magnetism and Magnetic Materials*, vol. 374, pp. 569-576, 2015.

[18] N. Bachok, A. Ishak, and I. Pop, "Unsteady boundary-layer flow and heat transfer of a nanofluid over a permeable stretching/shrinking sheet," *International Journal of Heat and Mass Transfer*, vol. 55, no. 7, pp. 2102-2109, 2012.

[19] P. Kameswaran, M. Narayana, P. Sibanda, and P. Murthy, "Hydromagnetic nanofluid flow due to a stretching or shrinking sheet with viscous dissipation and chemical reaction effects," *International Journal of Heat and Mass Transfer*, vol. 55, no. 25, pp. 7587-7595, 2012.

[20] D. Pal, G. Mandal, and K. Vajravelu, "MHD convection–dissipation heat transfer over a non-linear stretching and shrinking sheets in nanofluids with thermal radiation," *International Journal of Heat and Mass Transfer*, vol. 65, pp. 481-490, 2013.

[21] D. Pal and G. Mandal, "Hydromagnetic convective–radiative boundary layer flow of nanofluids induced by a non-linear vertical stretching/shrinking sheet with viscous–Ohmic dissipation," *Powder Technology*, vol. 279, pp. 61-74, 2015.

[22] M. Uddin, O. A. Bég, and N. Amin, "Hydromagnetic transport phenomena from a stretching or shrinking nonlinear nanomaterial sheet with Navier slip and convective heating: a model for bio-nano-materials processing," *Journal of Magnetism and Magnetic Materials*, vol. 368, pp. 252-261, 2014.

[23] N. Freidoonimehr, M. M. Rashidi, and S. Mahmud, "Unsteady MHD free convective flow past a permeable stretching vertical surface in a nano-fluid," *International Journal of Thermal Sciences*, vol. 87, pp. 136-145, 2015.

[24] K. Jafar, R. Nazar, A. Ishak, and I. Pop, "MHD flow and heat transfer over stretching/shrinking sheets with external magnetic field, viscous dissipation and Joule effects," *The Canadian Journal of Chemical Engineering*, vol. 90, no. 5, pp. 1336-1346, 2012.

[25] N. A. Haroun, P. Sibanda, S. Mondal, and S. S. Motsa, "On unsteady MHD mixed convection in a nanofluid due to a stretching/shrinking surface with suction/injection using the spectral relaxation method," *Boundary value problems*, vol. 2015, no. 1, p. 24, 2015.

[26] M. Miklavcic and C. Wang, "Viscous flow due to a shrinking sheet," *Quarterly of Applied Mathematics*, vol. 64, no. 2, pp. 283-290, 2006.

[27] C. Wang, "Stagnation flow towards a shrinking sheet," *International Journal of Non-Linear Mechanics*, vol. 43, no. 5, pp. 377-382, 2008.

[28] S. Nadeem and R. Ul Haq, "MHD boundary layer flow of a nanofluid passed through a porous shrinking sheet with thermal radiation," *Journal of Aerospace Engineering*, vol. 28, no. 2, p. 04014061, 2012.

[29] R. Haq, S. Nadeem, Z. Khan, and T. Okedayo, "Convective heat transfer and MHD effects on Casson nanofluid flow over a shrinking sheet," *Open Physics*, vol. 12, no. 12, pp. 862-871, 2014.

[30] A. M. Rohni, S. Ahmad, and I. Pop, "Flow and heat transfer over an unsteady shrinking sheet with suction in nanofluids," *International Journal of Heat and Mass Transfer*, vol. 55, no. 7, pp. 1888-1895, 2012.

[31] A. M. Rohni, S. Ahmad, A. I. M. Ismail, and I. Pop, "Flow and heat transfer over an unsteady shrinking sheet with suction in a nanofluid using Buongiorno's model," *International Communications in Heat and Mass Transfer*, vol. 43, pp. 75-80, 2013.

[32] M. H. M. Yasin, A. Ishak, and I. Pop, "MHD heat and mass transfer flow over a permeable stretching/shrinking sheet with radiation effect," *Journal of Magnetism and Magnetic Materials*, vol. 407, pp. 235-240, 2016.

[33] J. Merkin and V. Kumaran, "The unsteady MHD boundary-layer flow on a shrinking sheet," *European Journal of Mechanics-B/Fluids*, vol. 29, no. 5, pp. 357-363, 2010.

[34] K. Bhattacharyya, "Effects of radiation and heat source/sink on unsteady MHD boundary layer flow and heat transfer over a shrinking sheet with suction/injection," *Frontiers of Chemical Science and Engineering*, vol. 5, no. 3, pp. 376-384, 2011.

[35] A. Kuznetsov and D. Nield, "The Cheng–Minkowycz problem for natural convective boundary layer flow in a porous medium saturated by a nanofluid: a revised model," *International Journal of Heat and Mass Transfer*, vol. 65, pp. 682-685, 2013.

[36] T. Cebeci and P. Bradshaw, *Physical and computational aspects of convective heat transfer*. Springer Science & Business Media, 2012.

[37] W. Ibrahim and B. Shankar, "MHD boundary layer flow and heat transfer of a nanofluid past a permeable stretching sheet with velocity, thermal and solutal slip boundary conditions," *Computers & Fluids*, vol. 75, pp. 1-10, 2013.

[38] Y. S. Daniel, "Laminar Convective Boundary Layer Slip Flow over a Flat Plate using Homotopy Analysis Method," *Journal of The Institution of Engineers (India): Series E*, vol. 97, no. 2, pp. 115-121, 2016.

[39] Y. S. Daniel, Z. A. Aziz, Z. Ismail, and F. Salah, "Impact of thermal radiation on electrical MHD flow of nanofluid over nonlinear stretching sheet with variable thickness," *Alexandria Engineering Journal*, 2017. https://doi.org/10.1016/j.aej.2017.07.007

[40] Y. S. Daniel, "Steady MHD Boundary-layer Slip Flow and Heat Transfer of Nanofluid over a Convectively Heated of a Non-linear Permeable Sheet," *Journal of Advanced Mechanical Engineering*, vol. 3, no. 1, pp. 1-14, 2016.

[41] Y. S. Daniel, Z. A. Aziz, Z. Ismail, and F. Salah, "Numerical study of Entropy analysis for electrical unsteady natural magnetohydrodynamic flow of nanofluid and heat transfer," *Chinese Journal of Physics*, vol. 55, no. 5, pp. 1821-1848, 2 017.

[42] K. Bhattacharyya, "Effects of heat source/sink on MHD flow and heat transfer over a shrinking sheet with mass suction," *Chemical Engineering Research Bulletin*, vol. 15, no. 1, pp. 12-17, 2011.

[43] R. Dhanai, P. Rana, and L. Kumar, "Multiple solutions of MHD boundary layer flow and heat transfer behavior of nanofluids induced by a power-law stretching/shrinking permeable sheet with viscous dissipation," *Powder Technology*, vol. 273, pp. 62-70, 2015.



**Yahaya Shagaiya Daniel** is currently Ph.D student in Applied Mathematics, Department of Mathematical Sciences, Universiti Teknologi Malaysia (UTM), Johor, Malaysia.

Zainal Abdul Aziz graduated Ph.D in Applied Mathematics, 1997, Universiti Kebangsaan Malaysia (UKM), Bangi, Malaysia and is currently Professor at the Department of Mathematical Sciences, UTM and Director of UTM Centre for Industrial and Applied Mathematics (UTM-CIAM),

Institute Ibnu Sina for Scientific and Industrial Research, UTM, Johor, Malaysia.
Zuhaila Ismail graduated Ph.D in Applied Mathematics, 2013, University of Southampton, Southampton, United Kingdom and is currently Senior Lecturer at the Department of Mathematical Sciences and a fellow of UTM-CIAM, Universiti Teknologi Malaysia (UTM), Johor, Malaysia.
Faisal Salah graduated Ph.D in Applied Mathematics, 2012, Universiti Teknologi Malaysia (UTM), Johor, Malaysia and is currently Assoc. Prof. at the Department of Mathematics, University of Kordofan, Elobied, Sudan.